


# Impact of springtime Himalayan–Tibetan Plateau snowpack on the onset of the Indian summer monsoon in coupled seasonal forecasts

Retish Senan<sup>1,2</sup>  · Yvan J. Orsolini<sup>3,4</sup> · Antje Weisheimer<sup>5,6</sup> · Frédéric Vitart<sup>5</sup> · Gianpaolo Balsamo<sup>5</sup> · Timothy N. Stockdale<sup>5</sup> · Emanuel Dutra<sup>5</sup> · Francisco J. Doblas-Reyes<sup>7,8,9</sup> · Droma Basang<sup>10,11</sup>

Received: 1 July 2015 / Accepted: 14 January 2016 / Published online: 20 February 2016  
© The Author(s) 2016. This article is published with open access at Springerlink.com

**Abstract** The springtime snowpack over the Himalayan–Tibetan Plateau (HTP) region and Eurasia has long been suggested to be an influential factor on the onset of the Indian summer monsoon. To assess the impact of realistic initialization of springtime snow over HTP on the onset of the Indian summer monsoon, we examine a suite of coupled ocean–atmosphere 4-month ensemble reforecasts made at the European Centre for Medium-Range Weather Forecasts, using

their Seasonal Forecasting System 4. The reforecasts were initialized on 1 April every year for the period 1981–2010. In these seasonal reforecasts, the snow is initialized “realistically” with ERA-Interim/Land Reanalysis. In addition, we carried out an additional set of forecasts, identical in all aspects except that initial conditions for snow-related land surface variables over the HTP region are randomized. We show that high snow depth over HTP influences the meridional tropospheric temperature gradient reversal that marks the monsoon onset. Composite difference based on a normalized HTP snow index reveal that, in high snow years, (1) the onset is delayed by about 8 days, and (2) negative precipitation anomalies and warm surface conditions prevail over India. We show that about half of this delay can be attributed to the realistic initialization of snow over the HTP region. We further demonstrate that high April snow depths over HTP are not uniquely influenced by El Niño–Southern Oscillation, the Indian Ocean Dipole or the North Atlantic Oscillation.

**Electronic supplementary material** The online version of this article (doi:10.1007/s00382-016-2993-y) contains supplementary material, which is available to authorized users.

✉ Retish Senan  
retish.senan@geo.uio.no

- <sup>1</sup> Department of Geosciences, University of Oslo, P. O. Box 1022, 0315 Blindern, Oslo, Norway
- <sup>2</sup> Present Address: European Centre for Medium-Range Weather Forecasts, Reading, UK
- <sup>3</sup> Norwegian Institute for Air Research (NILU), Kjeller, Norway
- <sup>4</sup> Bjerknes Centre for Climate Research, Bergen, Norway
- <sup>5</sup> European Centre for Medium-Range Weather Forecasts, Reading, UK
- <sup>6</sup> Department of Physics, UK National Centre for Atmospheric Science (NCAS), University of Oxford, Oxford, UK
- <sup>7</sup> Institució Catalana de Recerca i Estudis Avançats (ICREA), Barcelona, Spain
- <sup>8</sup> Barcelona Supercomputing Center-Centro Nacional de Supercomputación (BSC-CNS), Barcelona, Spain
- <sup>9</sup> Institut Català de Ciències del Clima (IC3), Barcelona, Spain
- <sup>10</sup> Geophysical Institute, University of Bergen, Bergen, Norway
- <sup>11</sup> Institute of Tibetan Plateau Atmospheric and Environmental Science Research, Lhasa, Tibet, China

**Keywords** Indian monsoon · Seasonal forecasting · Monsoon onset · Land–atmosphere interactions · Snow depth

## 1 Introduction

The Indian Summer Monsoon (ISM) is one of the climate phenomena with the strongest social and economic impact, and affects one of the most densely populated parts of the world. The ISM is a manifestation of the coupled ocean–atmosphere–land system, influenced by high orography. While total seasonal rainfall and its intra-seasonal variability in the active and break periods often have the largest societal impacts, the monsoon onset is nevertheless a date that significantly affects human activities over the Indian

peninsula. Hence, the prediction of monsoon onset and rainfall has been an important research activity for decades (e.g., Webster et al. 1998; Krishnamurti et al. 2006; Turner and Annamalai 2012; Goswami and Krishnan 2013).

While visibly manifested as a rapid and intense spell of rainfall over the Indian sub-continent, at a fundamental level however, the monsoon onset is marked by the seasonal reversal of the meridional tropospheric temperature gradient (TTG) over the Indian monsoon region (Li and Yanai 1996; Xavier et al. 2007). The north–south gradient switches from a negative to a positive value at the monsoon onset resulting mainly from the deep tropospheric heating over the Himalayan and Tibetan Plateau (HTP) region during the pre-monsoon period (April–May, Yanai and Wu 2006), which is faster than on oceanic areas to the south (Dai et al. 2013). This land heating allows conditions favourable for the northward migration of convection regions, away from the equator.

The first suggestion of an inverse relationship between the springtime Himalayan snowpack and subsequent rainfall over the Indian sub-continent was hypothesized by Blanford (1884). The current reasoning and the physical basis for this Blanford hypothesis would be that a thick snowpack over the HTP region would have a local feedback effect. Snow-covered land can influence the above-lying atmosphere because of its remarkable insulating and reflecting properties and of the snowpack role in the hydrological cycle (e.g., Cohen and Entekhabi 2001; Xu and Dirmeyer 2011; Orsolini et al. 2013). Excessive snow cover due to its high reflectance, reduces net solar radiation and thereby decreases the land surface temperature (snow-albedo effect). Also, excessive snow accumulation during winter and spring leads to colder surface temperature as a significant portion of the incoming solar radiation is used up in melting the snow pack and evaporating cooling of the resultant soil moisture (snow-hydrology effect). Further, a thick snow pack insulates the overlying air from the soil layer below (snow-thermodynamic effect). The net resultant decrease in the surface sensible heating of the overlying air, and thus the reduced deep heating of the troposphere, weakens the TTG, delaying the ISM onset.

The first study on the HTP snow-monsoon linkage in the modern era was the observational study of Hahn and Shukla (1976). Using satellite imagery, they found an inverse relation between Eurasian winter snow cover and the Indian summer monsoon rainfall (ISMR) based on only 9 years of data. Dickson (1984) substantiated the above study with an additional 5 years of data and extended the result to the Himalayan region. Kripalani et al. (2003) also used satellite snow cover data for 1986–2000 and found that the inverse relationship between spring snow cover and ISMR remained robust. Saha et al. (2013) focused on mid and high latitudes and found a correlation between ISMR and an east–west dipole pattern in snow depth across Eurasia in the

assimilated European Space Agency (ESA) GlobSnow dataset. Concordant conclusions on a high snow/delayed ISM linkage were not found in all observational studies. Bamzai and Shukla (1999) used 22 years of satellite-derived snow-cover data but found no significant correlation between Himalayan seasonal snow cover and ISMR. Robock (2003) found higher than normal Tibetan snow cover in winter and spring preceding strong ISM rainfall. Hence, differences remain, depending on whether snow depth or snow cover was considered, and on the nature of the snow observations.

Several modeling studies have also addressed the Blanford hypothesis and tried to identify a snow-monsoon relationship, but again with mixed results. Peings and Douville (2010) could not find a definite and consistent relationship between Himalayan snow cover and the ISM in the different CMIP3 model simulations. However, Fasullo (2004) confirmed the Blanford mechanism during non-ENSO years, but noted that ENSO overwhelmed the influence of snow in other years. Turner and Slingo (2011) and Saha et al. (2013) demonstrated that snow forcing reduced tropospheric heating and weakened the monsoon development. In particular, Turner and Slingo (2011) found that the effect of snow-albedo feedback was the major contributor to tropospheric cooling over the HTP and thereby more critical to the Blanford mechanism in their model than the snow-hydrology effect.

The implications of these studies for seasonal forecasting with modern dynamical prediction systems have been little explored. The skill of these systems in predicting the ISM onset is still limited (Cherchi and Navarra 2003; Li and Zhang 2009; Alessandri et al. 2015), although some progress has been made on prediction of June monsoon rainfall with monthly forecast systems (Vitart and Molteni 2009). Atmospheric GCMs generally tend to show an early mean onset of the monsoon (e.g., Wang et al. 2004), while most coupled GCMs have delayed onsets (e.g., Kripalani et al. 2007; Zhang et al. 2012; Sperber et al. 2013). Realistic initialization of the atmosphere has recently been shown to improve the simulation of early onset (Alessandri et al. 2015), impacting the forecasts up to about a month. For the purpose of further improving the subseasonal-to-seasonal prediction skill of state-of-the-art dynamical prediction systems, there has been renewed interest in tapping into the potential of the land surface, hence also in improving the initialization of the land component. The impact of realistic initialization of soil moisture on actual subseasonal-to-seasonal predictability of surface temperature and precipitation was investigated in the multi-model intercomparison, Global Land–Atmosphere Coupling Experiment (Koster et al. 2010; GLACE2, e.g., van den Hurk et al. 2012). The strategy consisted of carrying out a twin-set of historical, ensemble forecasts differing only in the soil moisture initialization. More recently, a few studies adopted the same strategy to investigate the impact of snow initialization (Jeong et al. 2013; Orsolini et al. 2013).

The aim of this paper is to investigate the impact of realistic snow initialization over the HTP region on predicting the onset of the ISM, and on verifying the Blanford hypothesis using a state-of-the-art seasonal forecasting system. In order to attribute monsoon onset changes to the snow initialization over the HTP region, we adopt a twin forecast strategy similar to the one used in GLACE2 (Koster et al. 2010), comparing an ensemble of forecasts with realistic initialization with another set where snow initial conditions over HTP are randomized and unrealistic.

## 2 Model, data and methodology

### 2.1 Forecast model

Our twin-set of experiments is based on the ECMWF Seasonal Forecasting System 4, which comprises the IFS atmospheric model coupled to the NEMO Ocean model with a data assimilation system. Compared to the previous System 3 (Stockdale et al. 2011), System 4 now includes a new land surface scheme (H-TESSSEL), a 1-layer snow model and land surface initialization (see Molteni et al. 2011 for more details). The key thermodynamical and radiative feedbacks arising from snow covered land are at least partly incorporated in H-TESSSEL, and the new snow scheme leads to a more effective insulation, and hence a further cooling of the near-surface atmosphere (Dutra et al. 2011) than the one previously used in the operational model. The first set of forecasts, which we call the realistic “Series 1” experiments, comprises the 4-month long 15-member ensemble simulations starting on 1 April each year for the period 1981–2010, part of the operational “System 4” seasonal historical reforecasts made at ECMWF.

We then performed a second 15-member ensemble simulation, hereafter Series 2, which is identical to Series 1 in all aspects except that that initial conditions (IC) for snow-related land surface variables over the HTP region (hereafter defined as 27°N–40°N, 70°E–100°E) are randomized in a systematic manner, using 1 April IC from years between 1981 and 2010. The randomized variables are snow depth, snow density, snow albedo, snow layer temperature, soil moisture, soil temperature and skin temperature. Both series have realistic initial atmospheric and oceanic states, derived from ERA-Interim reanalysis (Dee et al. 2011) and from ORA-S4 oceanic reanalysis (Balmaseda et al. 2013), respectively.

### 2.2 Land reanalysis and ancillary in situ data

The initial land states are derived from the ERA-Interim/Land reanalysis (Balsamo et al. 2015). ERA-Interim/Land is a global land surface reanalysis dataset based on a land-surface model forced with near-surface meteorological parameters from ERA-Interim. To assess the quality of snow depth from the ERA-Interim/Land reanalysis over HTP, we use available station data over that region for the period 1980–2009. Station data comprise observations of monthly maximum snow depth from 47 locations over the Tibetan plateau, provided by the Tibetan Meteorological Bureau in Lhasa. The stations are located mostly over the most accessible central and eastern part of the plateau, to the east of 85°E. They also tend to be located in inhabited valleys.

### 2.3 Snow index

Figure 1 shows the normalized time series of April monthly mean snow depth over the HTP region in the ERA-Interim/

**Fig. 1** Time series of normalized snow depth in April over the Himalayan–Tibetan Plateau (27°N–40°N, 70°E–100°E) from the ERA-Interim/Land reanalysis. The inset shows the time series of monthly snow depth (cm) in April averaged over 47 stations in the Tibetan plateau region (blue) and the corresponding, collocated snow depths from the ERA-Interim/Land reanalysis (red). The symbols over/below the bars denote the phase of the three major climatic modes that influences the ocean-atmospheric conditions over the Indian summer monsoon region, vis, ENSO (filled squares), IOD (filled triangles) and NAO (filled circles), in the preceding autumn or winter season

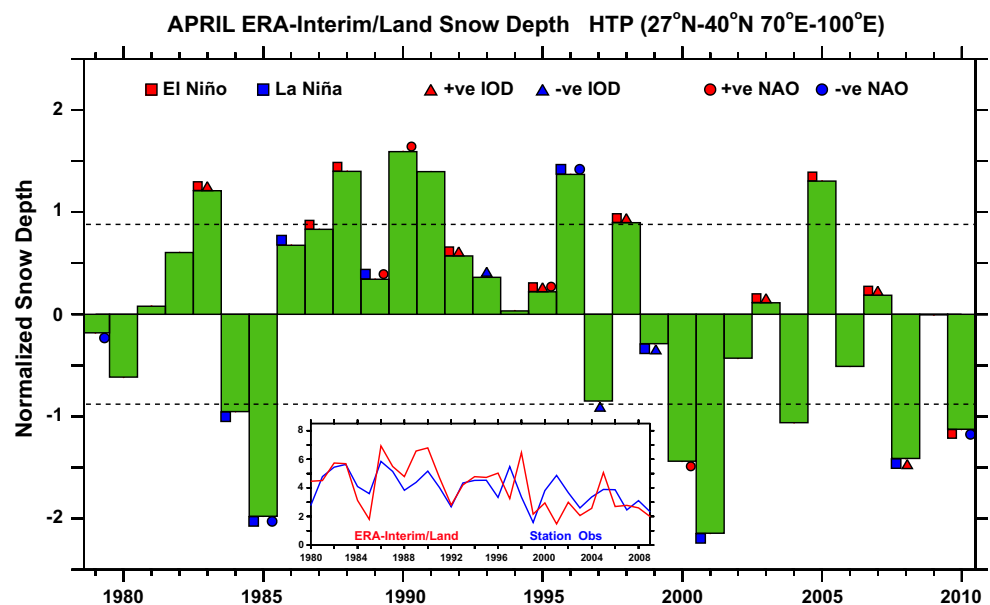


**Table 1** List of high and low snow years determined from snow depth over the HTP region based on the ERA-Interim/Land reanalysis (see Fig. 1)

High snow years	Low snow years
1983 (Jun 06)	1984 (May 19)
1988 (May 21)	1985 (May 21)
1990 (May 25)	2000 (May 18)
1991 (May 28)	2001 (May 23)
1996 (May 27)	2004 (May 21)
1998 (Jun 04)	2008 (May 19)
2005 (May 27)	2010 (May 25)

Date of monsoon onset in parentheses based on ERA-Interim reanalysis

Land data. The actual time series of snow depth (cm) averaged over the 47 stations and the corresponding average of collocated values from ERA-Interim/Land (after assigning proper weights for multiple station locations within the same reanalysis grid box) are also shown in the inset of Fig. 1. The correlation ( $r = 0.57$ ) between the two April time series is significant (at 99 %), indicating that the land reanalysis data has some realistic degree of skill at reproducing inter-annual variability. We focus on April, since the mean and variability of HTP snowpack remains large during that month, before decreasing sharply in May–June. Furthermore, April snow depth is a reflection of snow accumulation over the winter period and the HTP snow depth in April is highly correlated with earlier months. Composite analyses are performed based on the normalized April HTP snow depth (Fig. 1). The seven high and low snow years used in the composites correspond to an exceedance of 0.9 times the standard deviation and are listed in Table 1. A Monte-Carlo bootstrapping method consisting of 1000 random resampling of the field time-series at each grid point is used to test the significance of the composite fields. Glaciers in ERA-Interim and in the forecast model are represented by grid points with constant value of 10 cm of snow water equivalent. Such glaciers are masked before computing the area-averaged snow depth in our analysis.

## 2.4 Modelled mean monsoon

The fidelity of the forecast model in reproducing the main observed features of the climatological seasonal mean rainfall is assessed by comparing the model June to September mean precipitation with the Global Precipitation Climatology Project (GPCP) version 2.2 dataset (Adler et al. 2003) and the IMD gridded rainfall data (Pai et al. 2015) for the 1981–2010 period. The GPCP is a monthly precipitation dataset from 1979–present that combines in situ observations and satellite precipitation data into  $2.5^\circ \times 2.5^\circ$  global grids. The IMD data is based on daily station rain gauge data mapped onto a high

## JJAS Precipitation Climatology ( $\text{mm day}^{-1}$ ) 1981–2010

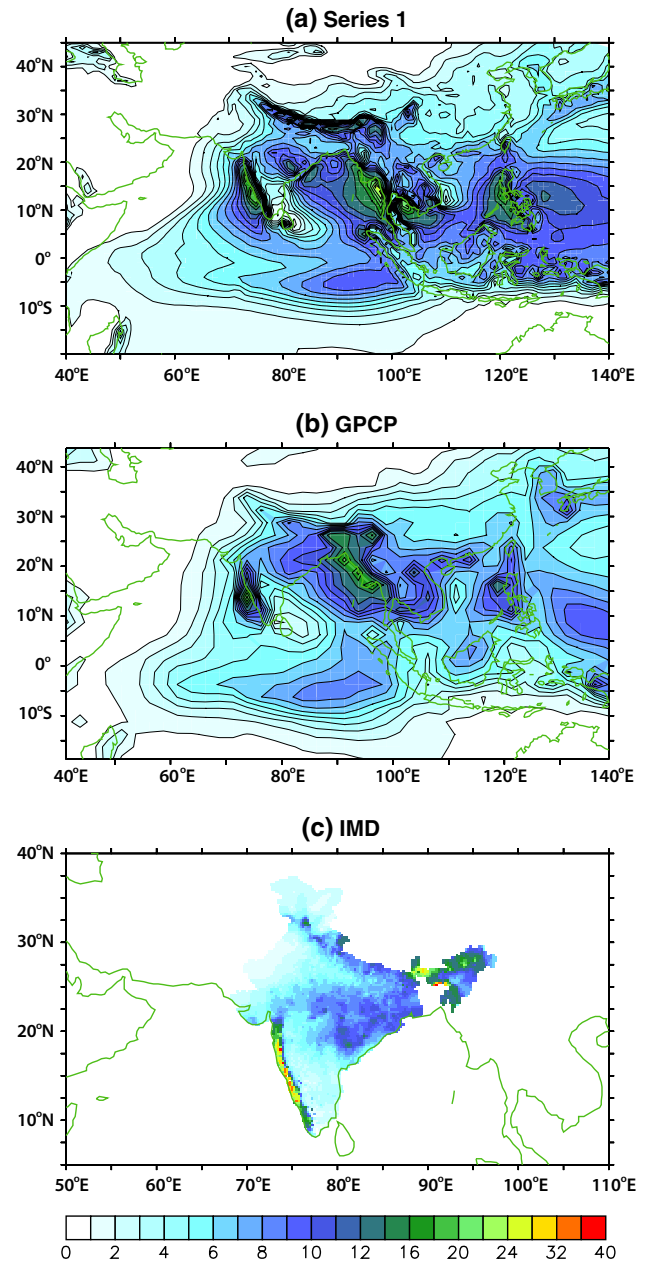


**Fig. 2** June to September mean precipitation climatology from **a** Series 1, **b** GPCP and **c** IMD gridded data for the 1981–2010 period

resolution  $0.25^\circ \times 0.25^\circ$  grid. The forecast model is in good comparison with GPCP and IMD (Fig. 2). The pattern of intense rainfall along the Western Ghats, the rainfall maxima over central-eastern India and the Himalayan belt, and the rain shadow region over eastern peninsular India seen in the forecast model is in good agreement with both the GPCP and the IMD products. Over the oceanic region, the pattern and magnitude of precipitation over the western Indian Ocean and the eastern equatorial Indian Ocean seen in GPCP are reasonably well reproduced by the forecast model.



**Table 2** Monsoon onset statistics for ERA-interim, Series 1 and Series 2

	ERA-interim	Series 1	Series 2
Mean onset date	May 29	May 26	May 25
High snow composite onset date	May 31	May 29	May 26
Low snow composite onset date	May 22	May 21	May 22
Onset difference (in days): high snow minus low snow years	9	8	4
Onset standard deviation	8.0	5.5	5.0

**Fig. 3** Time series of ensemble mean monsoon onset dates from the forecasts: Series 1 (blue) and Series 2 (red). Also plotted are the onset dates from ERA-Interim (green). The correlation between the forecasts and ERA-interim is shown

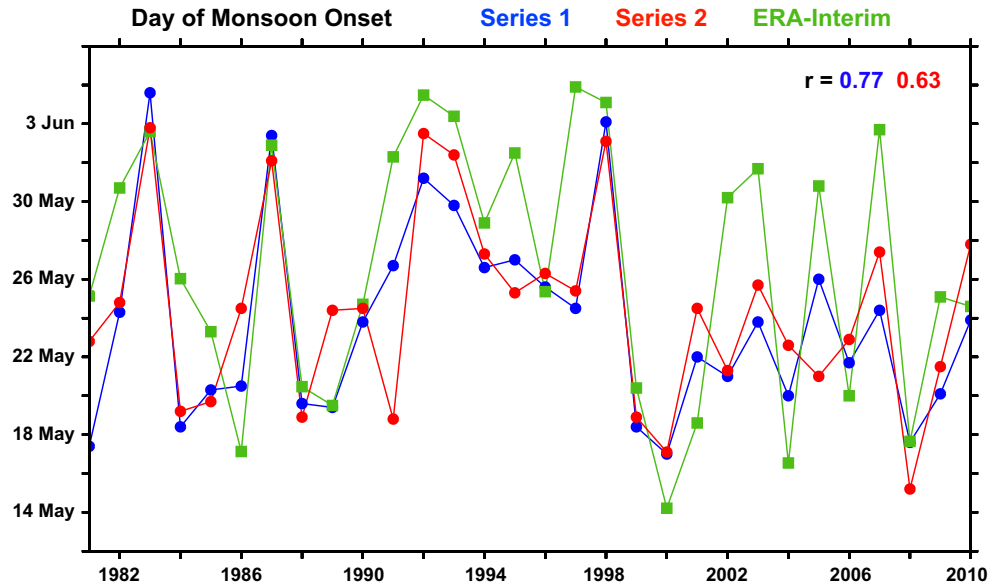
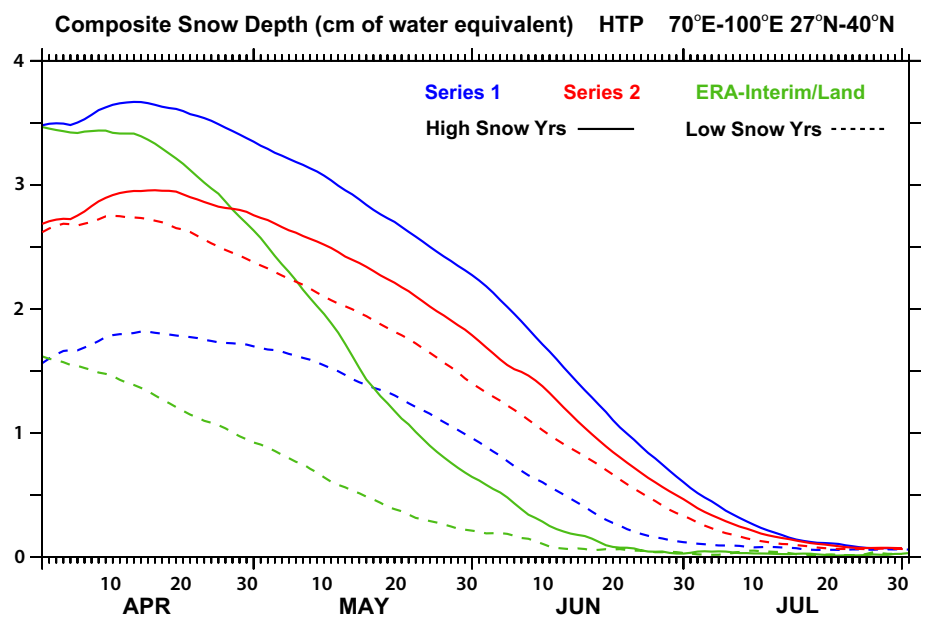


**Fig. 4** Daily time series of snow depth (cm of water equivalent) averaged over the HTP region composited over high snow (continuous line) and low snow (dashed line) years from Series 1 (blue) and the ERA-Interim/Land reanalysis (green). For Series 2, we consider the same years of high (low) snow but with low (high) unrealistic, randomized snow depths over HTP (red curves)



**2.5 Monsoon onset index**

In many studies, the ISM has been represented by the June-to-September mean of the All-India Rainfall, which is a

weighted average of rainfall over 29 meteorological subdivisions over India. The onset date has traditionally been determined based on arbitrary precipitation thresholds (e.g., Ananthkrishnan et al. 1967; Wang and LinHo 2002) and,

as noted by Xavier et al. (2007), such arbitrary representation of the monsoon rainfall can affect its inter-annual variability, and lead to bogus onsets (Flatau et al. 2001). Therefore, objective methods based on rainfall (Ananthakrishnan and Soman 1988) and large-scale dynamical indicators of the onset have been proposed (Fasullo and Webster 2003; Goswami and Xavier 2005; Wang et al. 2009). Furthermore,

since precipitation is still poorly modelled by forecast systems, an objective variable that is reasonably well reproduced by the models has to be selected (e.g., Alessandri et al. 2015). In this study, we are essentially looking at large scale and slowly evolving patterns, and therefore, we use the thermodynamic based definition of ISM onset following Xavier et al. (2007) and Prodhomme et al. (2015). This

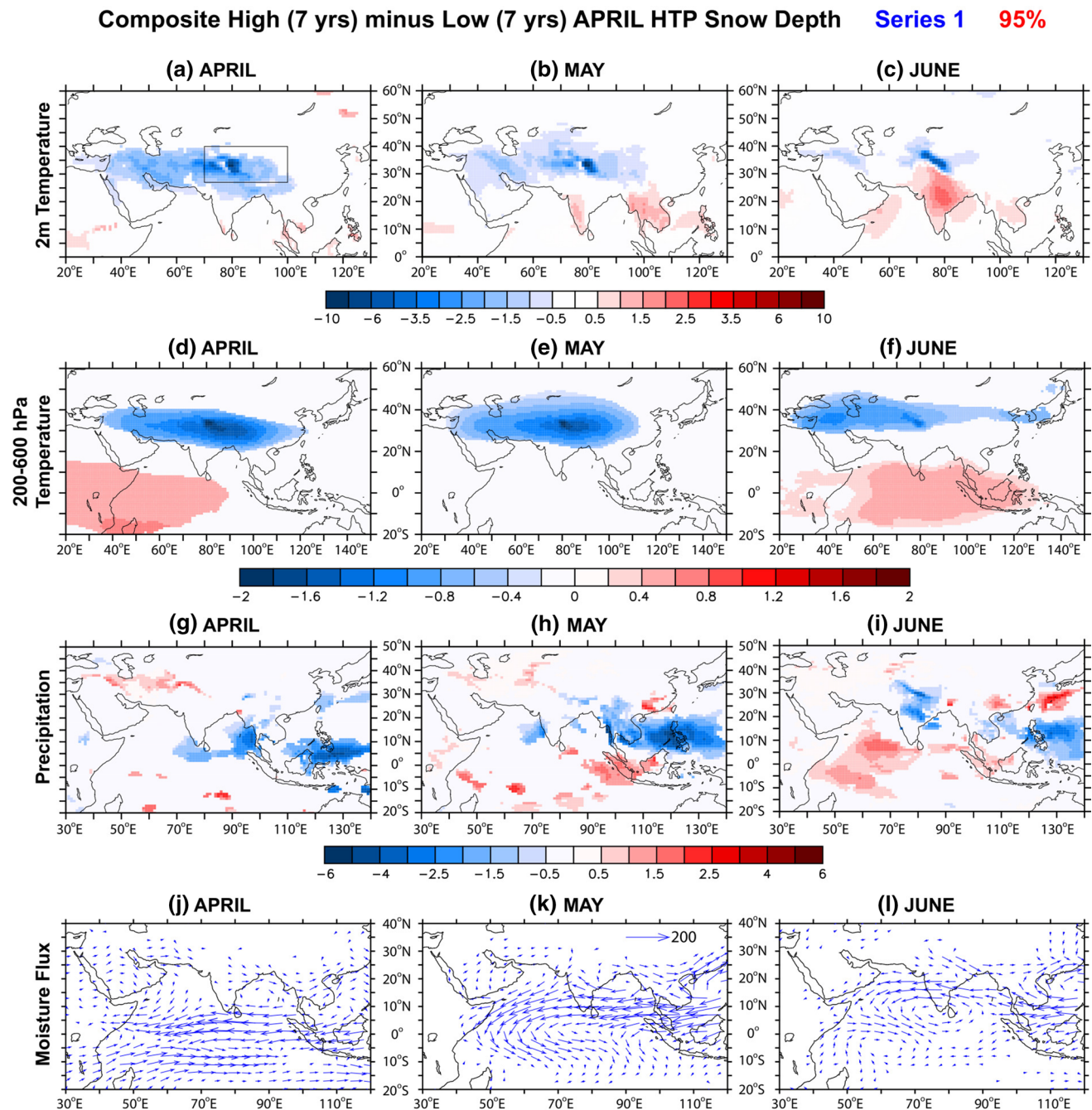


**Fig. 5** Composites of Series 1 monthly mean **a–c** 2 m temperature, **d–f** vertically integrated temperature between 200 and 600 hPa, **g–i** precipitation ( $\text{mm day}^{-1}$ ) and **j–l** vertically integrated moisture flux vectors ( $\text{kg m}^{-1} \text{s}^{-1}$ ), as a difference between high and low snow

years. Note that the map scale is different for the different variables. Only the 95 % significance levels (based on a Monte-Carlo bootstrapping method) are shaded in (**a–i**)

definition is based on the TTG reversal over the ISM region. The TTG is defined as the vertically integrated tropospheric (200–600 hPa) temperature difference, between a northern region (5°N–35°N) and southern region (15°S–5°N) over 40°E–100°E. The monsoon onset is defined as the day of the first change of sign of TTG from negative to positive with the sign remaining positive for at least 5 days to

prevent bogus onsets. The importance of incorporating the mid-tropospheric temperature variations was highlighted by Dai et al. (2013), who further compared the TTG diagnostic to other traditional indices based on vertical wind shear. The forecast model (Series 1) mean onset date (based on ensemble mean TTG) is 26<sup>th</sup> May, while in ERA-interim it is 29<sup>th</sup> May (Table 2), i.e. around 3 days later. We will come back

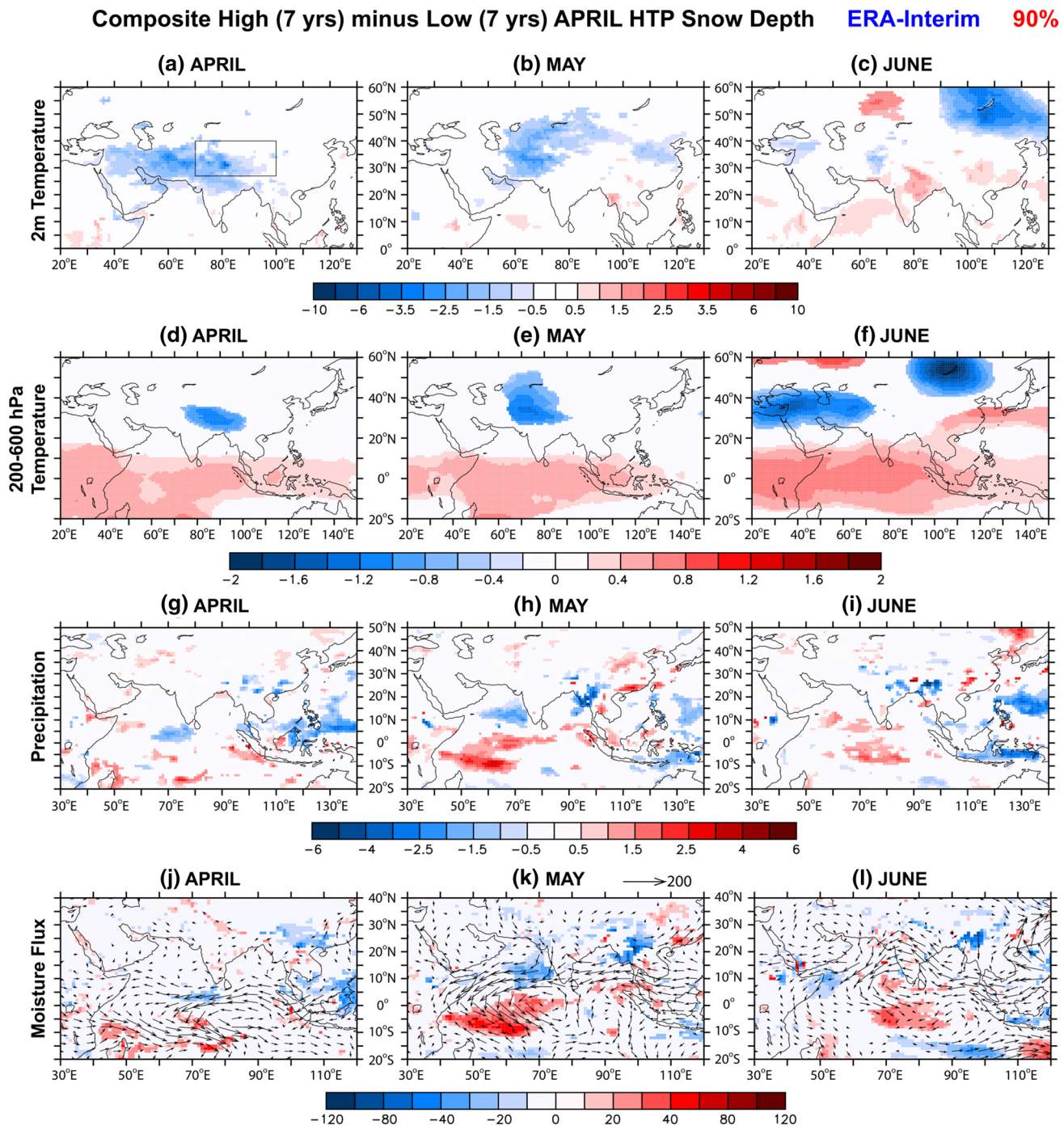


**Fig. 6** Same as Fig. 5 but for ERA-Interim at the 90 % significance level. The convergence of vertically integrated moisture flux is also shaded in (j–l)



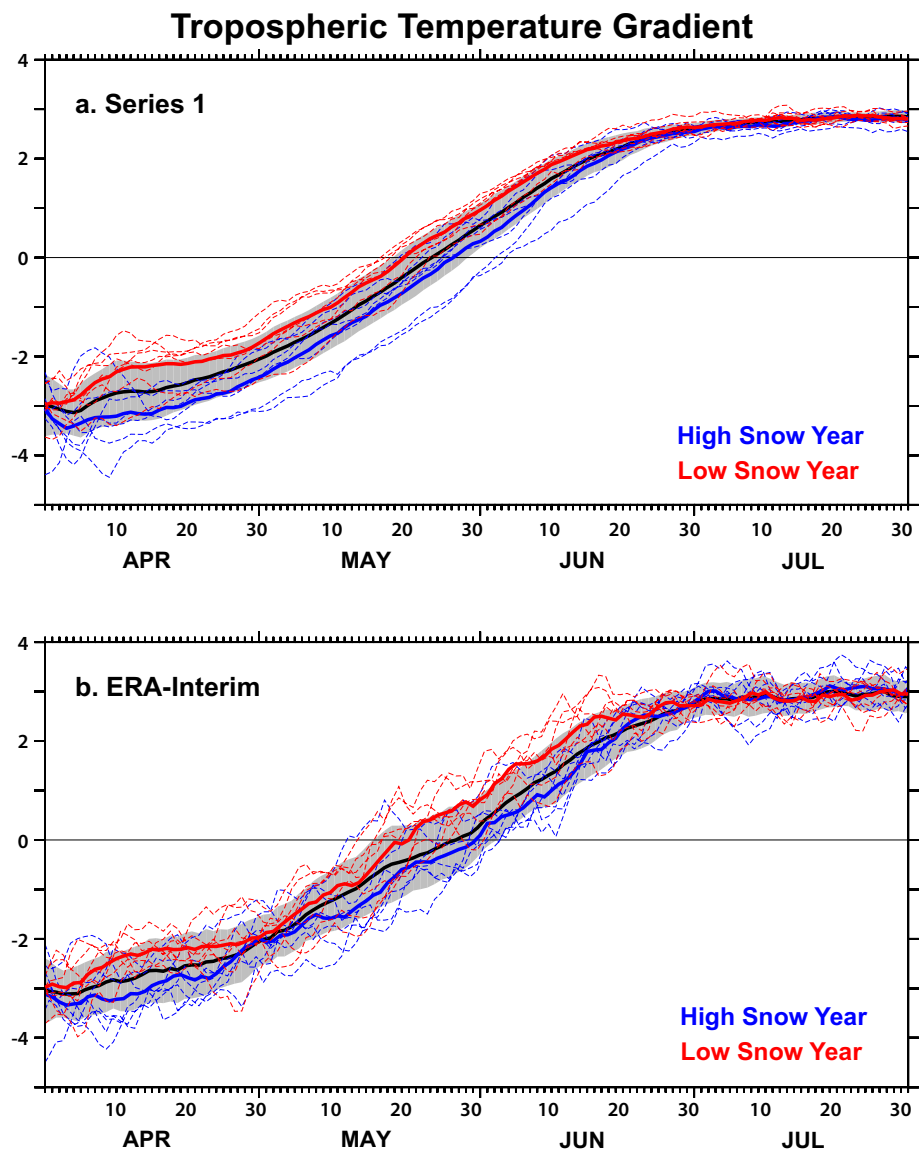
to this onset bias issue in Sect. 3. The onset inter-annual variability in the Series 1 is in good agreement with ERA-Interim (Fig. 3), with a significant correlation of 0.77. There is however, less variability in the forecast model onset in the last decade (2000s). Consequently, the standard deviation of the forecast model onset (5.5 days) is lower than that of ERA-Interim (8 days). Typical rainfall-based estimates of standard deviation vary between 5.5 to 9 days depending on the methodology used. The RMSE of onset day between Series 1 and ERA-Interim is around 5 days.

## 2.6 Climate patterns

Large scale modes of climate variability like ENSO, the Indian Ocean Dipole (IOD) and the North Atlantic Oscillation (NAO) could influence the snow depth over HTP in

spring. Indicators of such teleconnections are therefore calculated using the ERA-Interim reanalysis for the preceding autumn or winter season, when these modes peak. Thus, for ENSO, we use 5-month running mean SST anomaly in the preceding December over the Niño 3.4 region ( $120^{\circ}\text{W}$ – $170^{\circ}\text{W}$ ,  $5^{\circ}\text{S}$ – $5^{\circ}\text{N}$ ). Following Trenberth (1997), we define El Niño and La Niña years as those when the 5-month running mean SST in the Niño 3.4 region ( $120^{\circ}\text{W}$ – $170^{\circ}\text{W}$ ,  $5^{\circ}\text{S}$ – $5^{\circ}\text{N}$ ) exceeds  $+0.4^{\circ}\text{C}$  and  $-0.4^{\circ}\text{C}$  respectively. IOD is defined, following Saji et al. (1999), as the normalized SST anomaly difference between the western equatorial Indian Ocean ( $50^{\circ}\text{E}$ – $70^{\circ}\text{E}$ ,  $10^{\circ}\text{S}$ – $10^{\circ}\text{N}$ ) and the southeastern equatorial Indian Ocean ( $90^{\circ}\text{E}$ – $110^{\circ}\text{E}$ ,  $10^{\circ}\text{S}$ – $0^{\circ}\text{N}$ ) for the preceding September–October season. Positive (negative) IOD years are based on criteria that the normalized index is greater (lesser) than 0.8 ( $-0.8$ ) times the standard

**Fig. 7** Daily time evolution of the meridional tropospheric temperature gradient (TTG) over the Indian monsoon region in **a** Series 1 and **b** ERA-Interim for the different high snow (blue dashed) and low snow (red dashed) years and their composite mean (thick blue and red lines respectively). Also plotted are the climatological mean (thick black) and the envelope (grey shading) of one standard deviation spread for the 1981–2010 period





deviation. For NAO, we use an index based on normalized SLP anomaly difference between 65°N and 35°N averaged over the 80°W–30°E longitudinal band (after Li and Wang 2003) for the preceding winter (December–February). Positive (Negative) NAO years correspond to a normalized index greater (lesser) than 1.0 (−1.0) times the standard deviation.

### 3 Results

In order to gain insight into the spatial structure and evolution of the circulation anomalies associated with extremes of April snow over the HTP region, we first perform a composite analysis based on the normalized April HTP snow depth index, extending from the pre-monsoon and through the onset period (April to June).

#### 3.1 Composite time-evolution of HTP snow

The seasonal evolution of snow depth over HTP from the composited high and low snow years is shown in Fig. 4, for the Series 1 forecasts (blue curves) and for ERA-Interim/Land (green curves). We will comment on the curves for Series 2 later. We note the high bias in Series 1 after the initial date leading to an excessively persistent snowpack in both high and low snow years, which may indicate that the forecast model produces excessive snow depths compared to the ERA-Interim analysis used to drive ERA-Interim/Land.

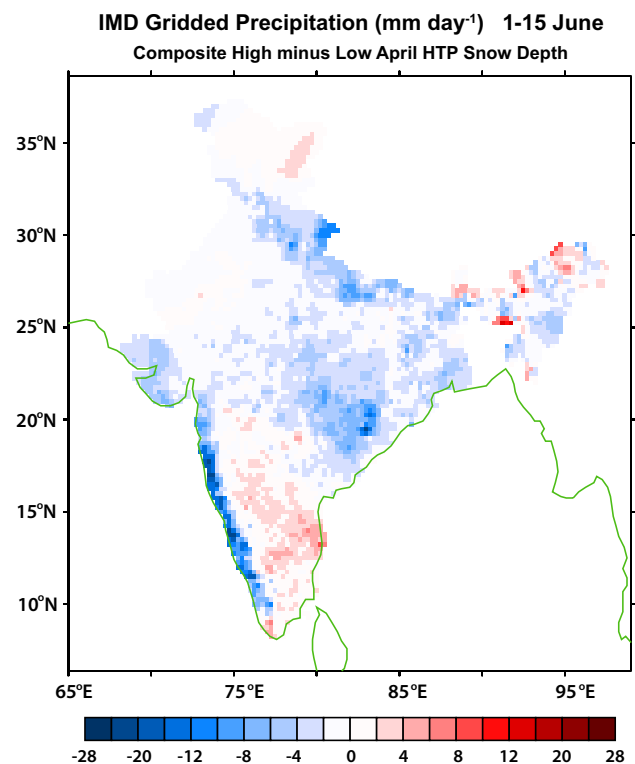
#### 3.2 Composite analysis of temperature, precipitation and moisture flux

Figure 5 shows the composite evolution of the difference of 2 m temperature between years of high and low April HTP snow depth in Series 1. Cold surface temperature anomalies persist over HTP and large surrounding areas in April (Fig. 5a). As the season progresses, the cooling area is more localized over the HTP region (Fig. 5b). This is consistent with an anomalously thick snowpack better insulating the atmosphere from the soil layers below (e.g., Dutra et al. 2011; Orsolini et al. 2013). It also increases the short-wave albedo at a time of year when solar radiation gets stronger, and both effects would lead to a cold surface anomaly. Not only does the increased snowpack in April reduce the sensible heating near the surface, but also the deep heating of the troposphere: the composite of the tropospheric temperature (200–600 hPa) shows a large region of cooling over the Tibetan Plateau and surrounding areas (Fig. 5d), which persists in May (Fig. 5e). Hence, the cold dome of air over the HTP region is reinforced by the presence of a thicker than normal snowpack. Interestingly however, warm surface temperature anomalies appear over

the Indian sub-continent in late May (Fig. 5b) that persist and strengthen in June (Fig. 5c). Precipitation composites shows negative precipitation anomalies covering the eastern Arabian Sea, along the west-coast of the Indian peninsula and most of Bay of Bengal in May (Fig. 5h) and spreads to the northern part of the Indian sub-continent by June (Fig. 5i). In summary, the negative precipitation anomalies and persisting dry and warm surface conditions over India indicate a delayed monsoon onset when the HTP snowpack in April is anomalously high.

Finally, moisture availability is analyzed using vertically integrated (from surface to 1 hPa) moisture flux vectors. The composite difference reveals an anomalous westward flux at low latitudes (e.g., 0–20°N), which indicates reduced moisture availability to the Indian sub-continent in May (Fig. 5k) since it opposes the climatological south-westerly monsoonal flux that brings moisture into the monsoon region.

Corresponding composite differences for ERA-Interim are shown in Fig. 6 and, in spite of the high model snow bias, the patterns are largely in agreement with the forecast model. The cold surface temperature anomalies in April over the HTP region (Fig. 6a), enhanced tropospheric cooling (Fig. 6d, e), reduced moisture availability (Fig. 6k) and



**Fig. 8** Composite of 1–15 June averaged IMD gridded precipitation ( $\text{mm day}^{-1}$ ) as a difference between high and low April HTP snow years for the 1981–2010 period

warm surface anomalies over the continent later in June (Fig. 6b) are consistent with the forecast model patterns. The precipitation pattern (Fig. 6g–i) shows some differences compared to the forecast model, and this is not unexpected given that precipitation is, in general, a difficult field to model (e.g., Sperber et al. 2013).

The delayed onset is further evident in the time series of the seasonal evolution of the ensemble-mean TTG (Fig. 7a), which shows that the monsoon onset, defined as the change of sign of the TTG, for the high snow years (blue lines) is clearly delayed with respect to the low snow years (red lines). The composite difference between the monsoon onset for the high snow and low snow years is about 8 days, which is significant at 95 % based on a Monte-Carlo bootstrapping method. Note that the onset time corresponds to a lead of about 2 months, as the forecasts start in April. The TTG values for high and low snow years are indistinguishable in the first few days of the simulation, and the separation between the high and low snow years starts after about 10 days. TTG from the ERA-Interim reanalysis (Fig. 7b) shows larger day-to-day and intra-seasonal variability for both the high and low snow years. The composite difference between the monsoon onset for the high snow and low snow years for ERA-Interim is about 9 days, close to the model value of around 8 days.

We have furthermore analyzed the daily, gridded IMD data set for the 1981–2010 period. We find that composite difference in rainfall for the first 2 weeks of June between years of high and low April HTP snow depth (Fig. 8) are consistent with the forecast model and reanalysis results: negative precipitation anomalies over most the south-western coast of India and over central and eastern parts of the sub-continent are indicative of a delayed monsoon onset. Over southeastern India, the composite difference shows a weak positive rainfall anomaly, which can be related to the enhanced westward flux of moisture (Fig. 5i), bringing moist oceanic air to the land. Furthermore, the composite of the total ISM rainfall for the 2 weeks of June for the high snow years (214.9 mm) is lower than that for the low snow years (295.9 mm).

### 3.3 Composite analysis of snow depth

A comparison of the April HTP snow depth time series (Fig. 1) and the monsoon onset time series (Fig. 3) show that not all high or low April HTP snow years show a one-to-one correspondence with late or early monsoon years. We find that 2 out of the 7 high snow years correspond to late onset and 3 out of the 7 late snow years correspond

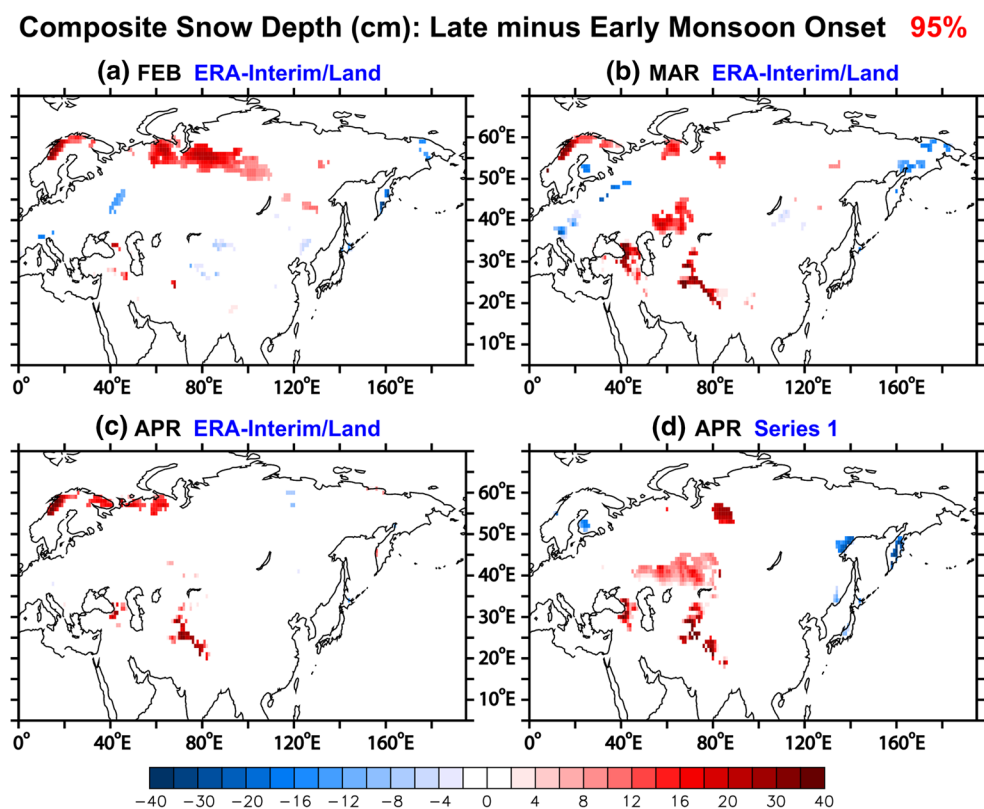


**Fig. 9** Composites of snow depth (cm) as a difference between late and early monsoon onset years. **a–c** ERA-Interim/Land from February to April and **d** Series 1 in April. Only the 95 % significance levels are shown

to early onset. However, the correlation between the April HTP snow and monsoon onset is 0.52 which is significant at 99 % based on a student  $t$  test. Therefore, to further confirm the relation between high HTP snow depth and delayed monsoon onset, we investigate the reciprocal snow-monsoon relation by performing a composite analysis of the snow depth based on early and late monsoon onset years. The composites are based on five early and late onset years corresponding to an exceedance of one standard deviation of the times series of forecast model onset date in Fig. 3. Large positive snow depth anomalies over the HTP region in spring (February–March–April, Fig. 9b, c) in ERA-Interim and in Series 1 in April (Fig. 9d) correspond to a delayed onset of the monsoon, confirming the relation found using the snow composites. There is also a region of positive snow depth anomaly over west central Eurasia in March in ERA-Interim and April in Series 1. However, we do not find an indication of the east–west dipole reported in some previous studies that have explored the relationship between the strength of the ISM rainfall and Eurasia snow cover (Peings and Douville 2010) or snow depths (Saha et al. 2013). It is to be noted that the central and northern Eurasian regions appear larger because of the distortion due to the map projection.

### 3.4 Impact of realistic snow over HTP

To assess the impact of realistic springtime HTP snow initial condition on the monsoon onset, we contrast Series 1 against the “unrealistic” Series 2. We perform composite analyses similar to Series 1 except that in Series 2, only members with snow depth IC values smaller (greater) than 0.5 times the climatological mean are used to calculate the ensemble mean for the high (low) snow years. This last step is to ensure that, in high snow years for example, we contrast Series 1 against an ensemble of low snow years from Series 2 and not another ensemble comprising also high snow years. The time evolution of composite HTP snow for the high and low snow years from Series 2 is shown as red curves in Fig. 2. Interestingly, we note a similar rebuilding of the snowpack in Series 2 (red solid line) as in Series 1, which indicates that the atmosphere is pre-conditioned for a snow build-up in high snow years.

The time series of onset dates from Series 2 shown in Fig. 3 has a lower correlation against ERA-Interim than Series 1 had. The RMSE of onset day between Series 2 and ERA-Interim is 5.5 days, larger when compared to Series 1. The mean onset date in Series 2 is May 25th (Table 2) and the corresponding composite difference between high and low snow years is 4 days, compared to 8 days in Series 1. Thus, according to our methodology, about half of the

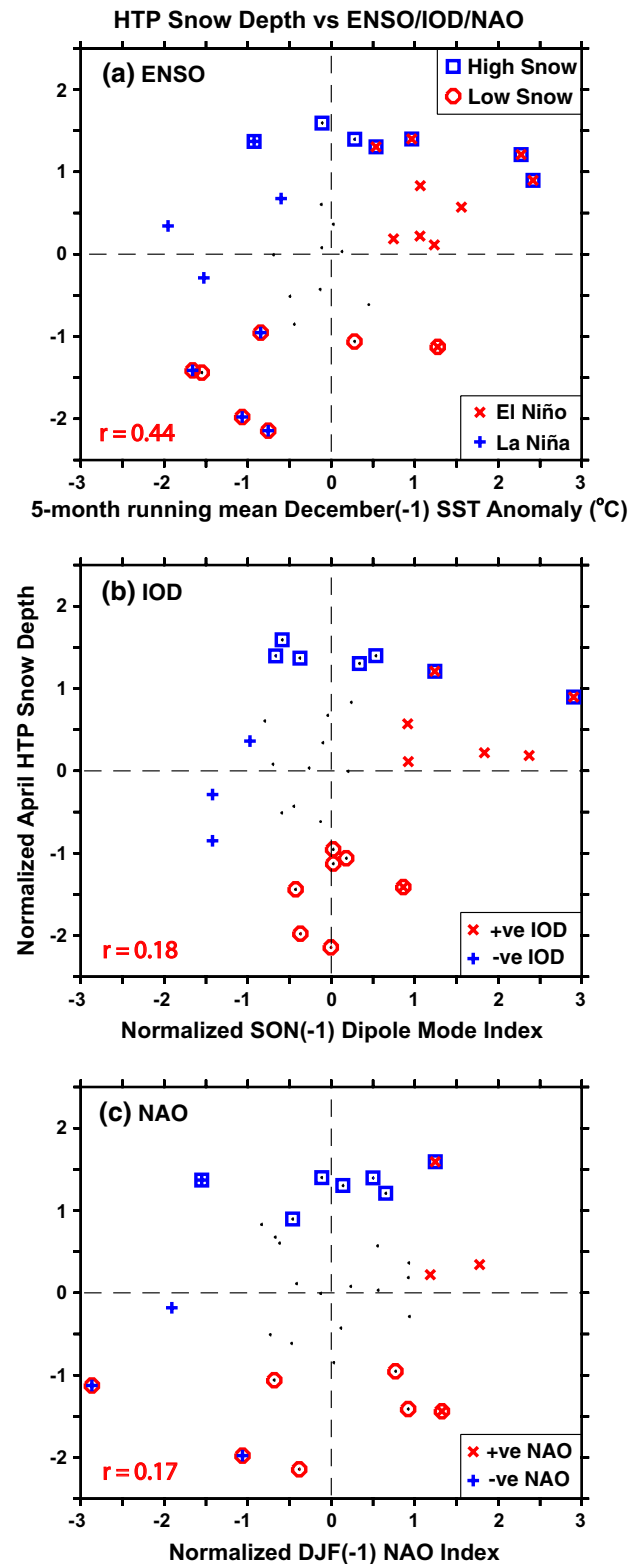


**Fig. 10** Scatter diagram of monthly means of normalized April HTP snow depth against **a** 5-month running mean December SST anomaly in the previous year over the Nino 3.4 region, **b** normalized IOD index for the September–November in the previous year and **c** normalized NAO index for December–January in the previous season

delay in monsoon onset is attributed to the impact of realistic snow initialization over the HTP region. The rest of the delay could arise from snow initialization elsewhere (e.g., in Eurasia), from the role of SSTs or from the atmospheric initial condition providing a pre-conditioning.

#### 4 Relation with global climate patterns

The fact that the high snow years with the two most pronounced delays of the ISM (1983, 1998) were preceded by El Niño events, warrants some further investigation of the links with ENSO, one of the largest factors influencing the ISM (e.g., Kumar et al. 2006), and with other large-scale teleconnection patterns. The question arises as to whether elevated April snow depths over HTP are linked to the ENSO phase in the preceding winter. Shaman and Tziperman (2005) found that El Niño could generate enhanced winter snowfall over HTP through a stationary wave and enhanced transient eddy activity. However, these results based on only 9 years of data were questioned by Yuan et al. (2009) who rather found that the IOD had a prevailing influence on HTP spring snow cover, inducing a quasi-stationary cyclonic anomaly and a strong southeasterly moisture flux into the region. Robock (2003) and Buermann et al. (2005) also suggested that the wintertime NAO/Arctic Oscillation influences spring snow depths over Eurasia.

In our study, only the ENSO index shows a significant correlation coefficient ( $r = 0.44$ , significant at 98 %) with April HTP snow depth, while those for IOD and NAO do not ( $r = 0.18$  and  $r = 0.17$ , respectively). Further, Fig. 10a

shows the scatterplot between normalized April HTP snow depth and the previously defined ENSO index. Four of the seven high snow April months are preceded by an El Niño (blue squares with red cross sign). However, there are also five instances of El Niño in neutral snow years (red crosses). Reciprocally, there are four low snow years co-occurring with La Niña (red circles with blue plus sign), yet there are also three instances of La Niña with neutral snow (blue plus sign) and one with high snow (blue square with blue plus sign). The scatterplot between the normalized April HTP snow depth and the IOD index (Fig. 10b) shows that only two of the seven high snow April months were preceded by a (positive) IOD event. There is also a low snow year preceded by a positive IOD event and a high snow year preceded by a negative IOD event. Returning to Fig. 1, we have plotted markings on top of the April HTP snow depths, indicating the phase of these three main climate patterns during the preceding autumn or winter. The 2 years (1983, 1998) with the most strongly delayed ISM (Fig. 5a) were preceded by an El Niño, but both these 2 years were also preceded by positive IOD conditions in the Indian Ocean (Fig. 1, red squares and triangles), with the 1997-98 IOD event being the strongest in recent decades. However, there are four other years with co-occurring El Niño and positive IOD in neutral snow years (Fig. 1, red squares and triangles). NAO doesn't seem to exert any particular influence on HTP snow either (Fig. 10c), e.g., there is one instance each of positive NAO preceding both a high snow year and a low snow year and one instance each of negative NAO preceding both a high snow year and a low snow year. This is consistent with Buermann et al. (2005)

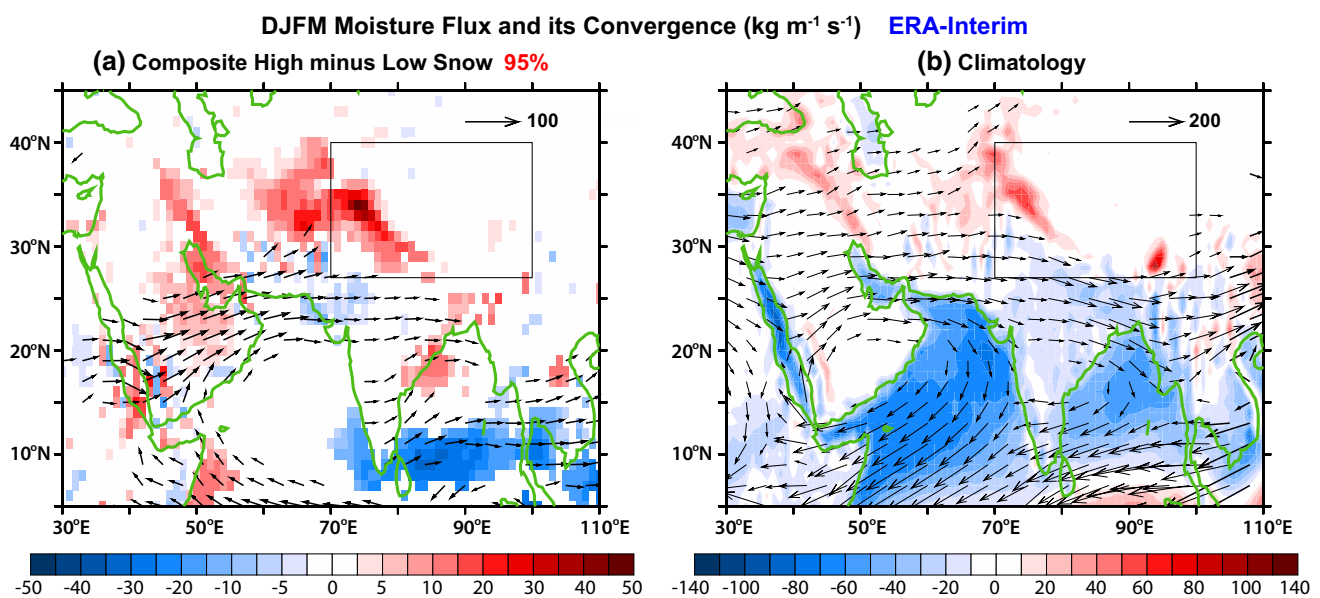


**Fig. 11** December to March averaged vertically integrated (surface to 1 hPa) moisture flux vectors and its convergence (*shaded*). **a** Composite difference between high and low HTP snow depth years and **b** Climatology over 1979–2010



who showed the winter NAO (or Arctic Oscillation) influenced springtime snow cover only over Eurasia at mid and high latitudes, to the north of the HTP region.

We have further analyzed the vertically integrated moisture flux into the monsoon region and its convergence during the winter (DJFM) preceding the anomalous HTP April snow depth, using the ERA-Interim reanalysis. The composite difference between high and low snow years is shown along with the climatology (Fig. 11a, b respectively). These figures reveal that moisture availability to the HTP region is largely influenced by the strengthening of the seasonal sub-tropical westerly jet over the Arabian Peninsula that results in more moisture inflow into the HTP region.

## 5 Discussion

### 5.1 Model snow bias

In this study, not only are the atmosphere and ocean realistically initialized but so is also the land component, and in particular snow depth. Following this realistic snow initialization, there is a positive model bias leading to excessive persistence of snow depth noted in Fig. 4, seen also in other regions like west and east Eurasia (not shown). However, this systematic bias does not affect our results since we are looking at composite differences. Further, the patterns and magnitudes of the high and low composites mirror each other when plotted separately rather than as a difference

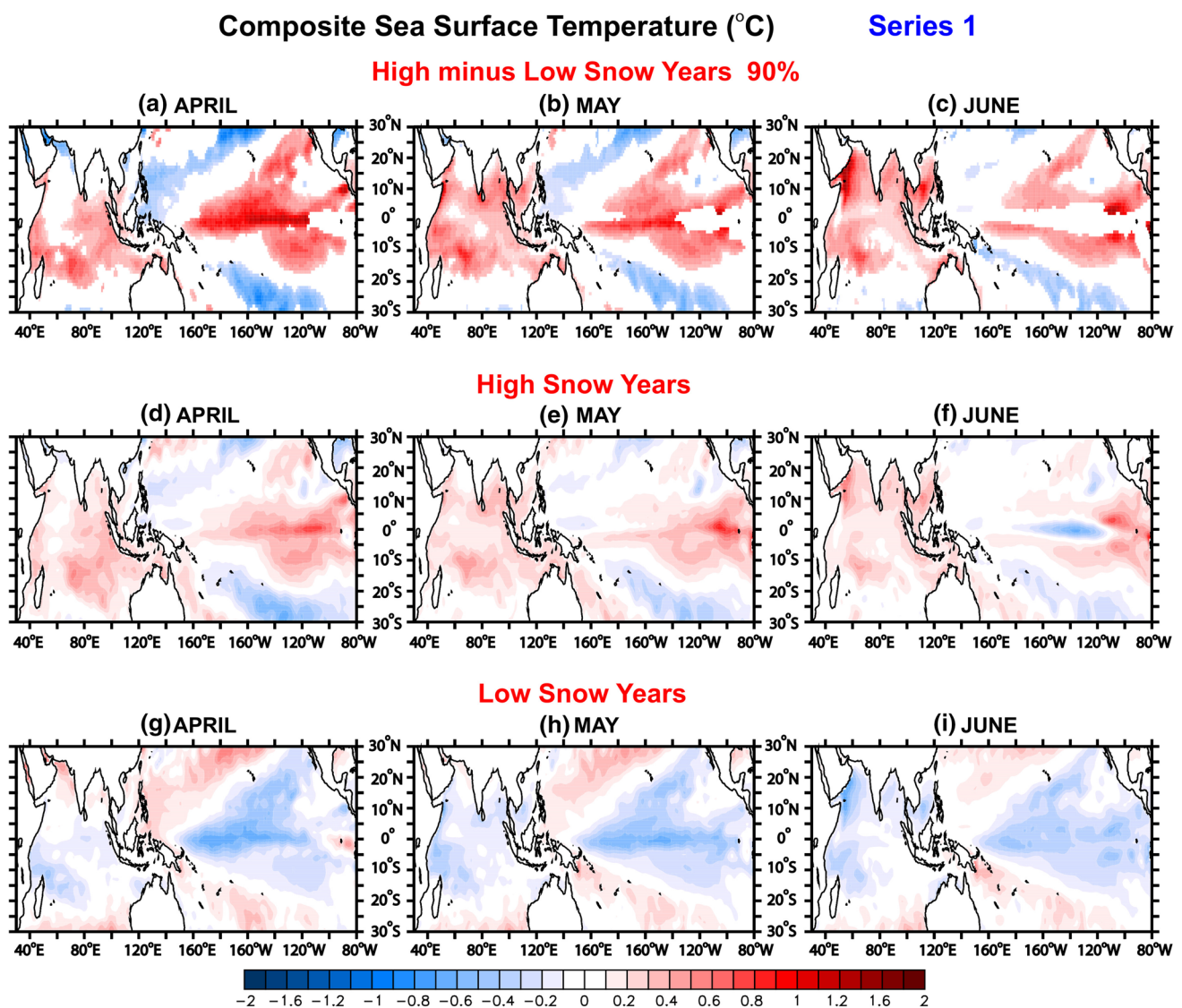


**Fig. 12** Composites of Series 1 monthly mean sea surface temperature for a–c high minus low HTP snow years d–f high snow years and g–i low snow years

(not shown). This implies that, in spite of the high snow bias, our results are robust.

## 5.2 ENSO and climate patterns

The wintertime moisture availability over the HTP (Fig. 11) is consistent with the April snow depths. While the majority (4 out of 7) of high (low) snow April months correspond to El Niño (La Niña), the occurrence of El Niño (La Niña) in preceding winter does not imply necessary high (low) April snow (4 out of 10, 3 out of 7, respectively). Hence, we have to conclude that snow conditions over HTP in April do not seem to be uniquely related to a particular phase nor a joint coincidence of the three examined climate patterns during the previous winter (ENSO, IOD and NAO). Either some additional climate phenomenon must be simultaneously

involved, or the ENSO influence could be random. The origin of the anomalous moisture fluxes in the subtropical or tropical region tentatively points to low latitude influence for this modulation. Further investigation of spring-time wave trains across Eurasia (e.g., Li et al. 2008) is also warranted.

## 5.3 SSTs

The delayed monsoon onset in coupled GCM's has been attributed to the role of warm SST biases in the Pacific Ocean (Prodhomme et al. 2015). Compared to ERA-Interim however, Series 1 forecasts show an early onset bias, which, in a corollary sense, could be related to the cold SST bias over most of the Pacific basin over the period 1981–2010 (Supplementary Fig. S1). The largest

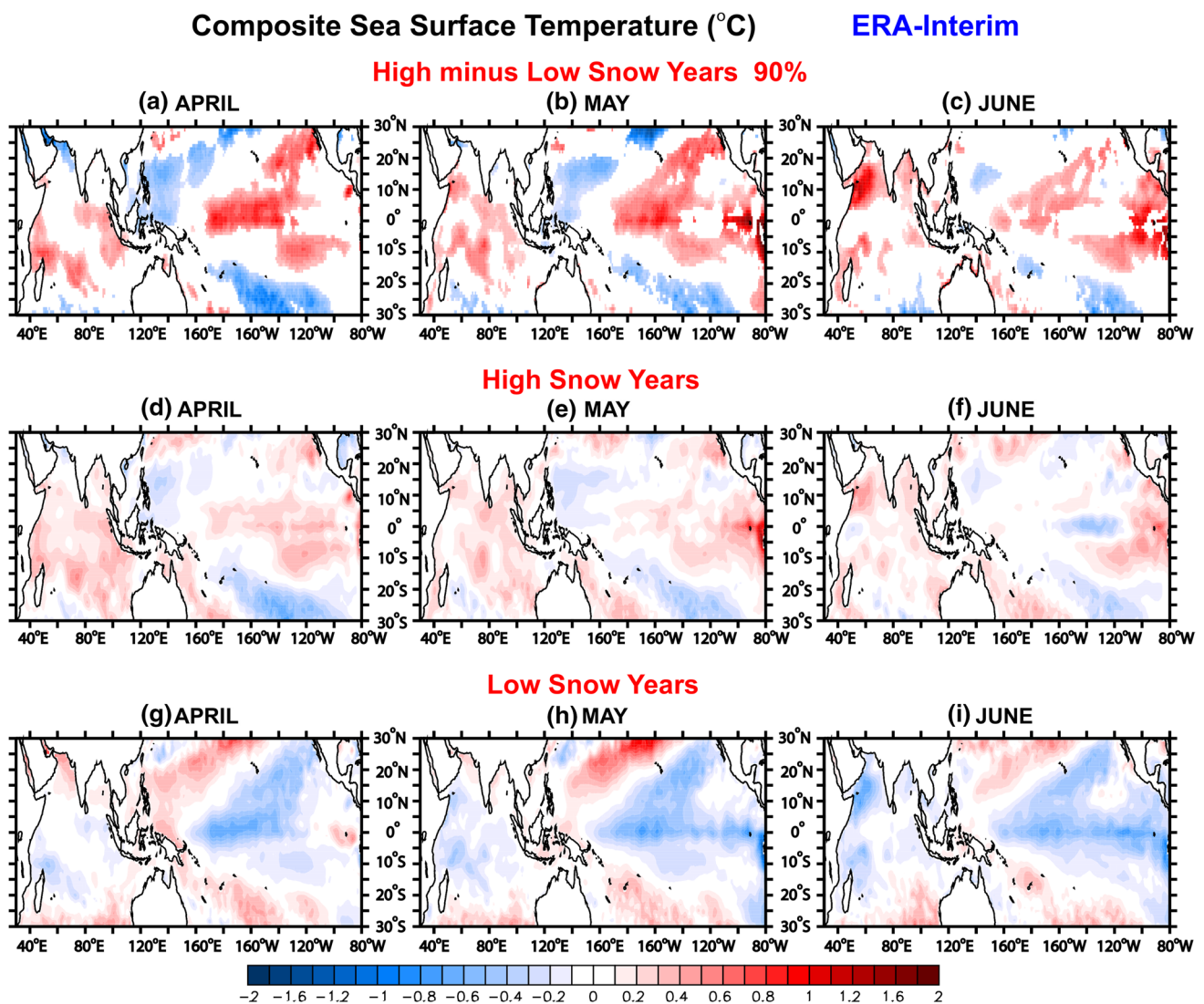


Fig. 13 Same as Fig. 12, but for ERA-interim

cold biases are confined to a narrow band in the eastern tropical Pacific in June (Fig. S1c). The cold bias over the Arabian Sea in May–June (Fig. S1b,c) is consistent with surface cooling due to upwelling resulting from biased (early and stronger) mean monsoonal flow and consequently the mean early onset bias. In spite of the mean bias, composite analysis of SST shows similar results for Series 1 and ERA-Interim. Composite SST difference between high and low HTP snow years for both Series 1 (Fig. 12a–c) and ERA-Interim (Fig. 13a–c) show significant warm anomalies over the Arabian Sea in May–June which is consistent with a weakened monsoonal flow. There are also significant warm anomalies in the Pacific. However, the composite SST patterns associated with high and low HTP snow conditions are not mirror of each other over the Pacific basin, while this is the case in the Indian Ocean. This is true not only in Series 1 but also in ERA-Interim. The low snow composites show a La Niña-type horseshoe pattern over the Pacific (Figs. 12g–i, 13g–i), whereas the high snow composites, while showing warm SST in the Pacific, is however not a typical El Niño like pattern (Figs. 12d–f, 13d–f). Thus, it appears that the influence of a preceding La Niña is longer-lived during low snow years compared to that of an El Niño during high snow years, the influence of which weakens by April (Figs. 12f, 13f).

#### 5.4 Summer intra-seasonal oscillation

The ISM evolution is affected by the boreal summer intra-seasonal oscillation (ISO). While its most notable manifestation is the active and break periods of the monsoon season, ISO can trigger the ISM onset and thereby modulate its inter-annual variability (e.g., Wheeler and Hendon 2004; Zhou and Murtugudde 2014). There are signatures of ISOs in the TTG from ERA-Interim (Fig. 6a). Individual forecast model members also display strong ISOs with phase and amplitude variations, but the ISOs are largely filtered out in the ensemble mean. The behavior of predicted ISOs is however beyond the scope of this study and could be better evaluated in medium-range forecasts (Fu et al. 2013). Since we are trying to delineate the impact on predictability of the slowly varying land surface, we are however interested in a mean delay of the onset and not in how individual ISO events trigger the onset.

## 6 Summary

In this study, the impact of snow initialization over the HTP region in springtime on the ISM onset was assessed in coupled seasonal forecasts with realistically initialized atmospheric, oceanic and land component. Composite

differences associated with inter-annual snow depth anomalies over HTP are in close agreement with those found using reanalysis (Figs. 3, 5, 6). Our results are consistent with the Blanford hypothesis—when the HTP snowpack in April is anomalously high, persisting dry and warm surface conditions and negative precipitation anomalies over India in May–June indicate a delayed monsoon onset. The contrast between an anomalously high versus low snowpack over the HTP region influences the tropospheric heating in pre-monsoon months, delays the reversal of the TTG and the onset of the monsoon by up to 8 days. A sensitivity experiment with unrealistic (randomized) snow initial condition over the HTP region indicates that about half of the delay can be attributed to the impact of snow over the HTP region. The rest of the delay could arise from snow initialization elsewhere (e.g., over Eurasia), from SSTs or from the atmospheric initial state conditioning the snowpack build-up. Dedicated experiments could be further tailored to individually assess the impact of these factors separately, albeit coupled simulations at this high spatial resolution are computationally demanding. Finally, as noted in Sect. 3.3, there is not a clear one-to-one correspondence between high (low) HTP snow and late (early) monsoon onset years. This indicates that there are multiple forcing factors and complex ocean-atmospheric processes associated with the ISM onset. However, the delay attributable to HTP snow (4 days) is of the order of the inter-annual variability in modelled ensemble-mean ISM onset (5.5 days). Thus, in spite of this caveat, HTP snow is an important component of the inter-annual variability of the monsoon. Further studies should be devoted to determine the sources of inter-annual to decadal variability of the springtime snowpack over the HTP region and potential teleconnections.

**Acknowledgments** RS and YOR were supported by the Research Council of Norway through the NORINDIA Project (#216576). AW and YOR were also supported by the EU project SPECS funded by the European Commission’s Seventh Framework Research Programme under the grant agreement 308378.

**Open Access** This article is distributed under the terms of the Creative Commons Attribution 4.0 International License (<http://creativecommons.org/licenses/by/4.0/>), which permits unrestricted use, distribution, and reproduction in any medium, provided you give appropriate credit to the original author(s) and the source, provide a link to the Creative Commons license, and indicate if changes were made.

## References

- Adler RF, Huffman GJ, Chang A et al (2003) The version-2 global precipitation climatology project (GPCP) monthly precipitation analysis (1979-present). *J Hydrometeorol* 4:1147–1167. doi:10.1175/1525-7541(2003)004<1147:TVGPCP>2.0.CO;2



- Alessandri A, Borrelli A, Cherchi A et al (2015) Prediction of Indian summer monsoon onset using dynamical subseasonal forecasts: effects of realistic initialization of the atmosphere. *Mon Weather Rev* 143:778–793. doi:10.1175/MWR-D-14-00187.1
- Ananthkrishnan R, Soman MK (1988) The onset of the southwest monsoon over Kerala: 1901–1980. *J Climatol* 8:283–296. doi:10.1002/joc.3370080305
- Ananthkrishnan R, Acharya U, Krishnan A (1967) On the criteria for declaring the onset of the southwest monsoon over Kerala. *Forecasting Manual, FMU Rep. IV-18.1*. India Meteorological Department, Pune, India
- Balmaseda MA, Mogenssen K, Weaver AT (2013) Evaluation of the ECMWF ocean reanalysis system ORAS4. *Q J R Meteorol Soc* 139:1132–1161. doi:10.1002/qj.2063
- Balsamo G, Albergel C, Beljaars A et al (2015) ERA-interim/land: a global land surface reanalysis data set. *Hydrol Earth Syst Sci* 19:389–407. doi:10.5194/hess-19-389-2015
- Bamzai AS, Shukla J (1999) Relation between Eurasian snow cover, snow depth, and the Indian summer monsoon: an observational study. *J Clim* 12:3117–3132. doi:10.1175/1520-0442(1999)012<3117:RBESCS>2.0.CO;2
- Blanford HF (1884) On the connexion of the Himalaya snowfall with dry winds and seasons of drought in India. *Proc R Soc Lond* 37:3–22. doi:10.1098/rpsl.1884.0003
- Buermann W, Lintner B, Bonfils C (2005) A wintertime Arctic oscillation signature on early-season Indian Ocean monsoon intensity. *J Clim* 18:2247–2269. doi:10.1175/JCLI3377.1
- Cherchi A, Navarra A (2003) Reproducibility and predictability of the Asian summer monsoon in the ECHAM4-GCM. Reproducibility and predictability of the Asian summer monsoon in the ECHAM4-GCM. *Clim Dyn* 20:365–379. doi:10.1007/s00382-002-0280-6
- Cohen J, Entekhabi D (2001) The influence of snow cover on northern hemisphere climate variability. *Atmos Ocean* 39:35–53. doi:10.1080/07055900.2001.9649665
- Dai A, Li H, Sun Y et al (2013) The relative roles of upper and lower tropospheric thermal contrasts and tropical influences in driving Asian summer monsoons. *J Geophys Res Atmospheres* 118:7024–7045. doi:10.1002/jgrd.50565
- Dee DP, Uppala SM, Simmons AJ et al (2011) The ERA-Interim reanalysis: configuration and performance of the data assimilation system. *Q J R Meteorol Soc* 137:553–597. doi:10.1002/qj.828
- Dickson RR (1984) Eurasian snow cover versus Indian Monsoon rainfall—an extension of the Hahn-Shukla results. *J Clim Appl Meteorol* 23:171–173. doi:10.1175/1520-0450(1984)023<0171:ESC VIM>2.0.CO;2
- Dutra E, Schär C, Viterbo P, Miranda PMA (2011) Land-atmosphere coupling associated with snow cover. *Geophys Res Lett* 38:L15707. doi:10.1029/2011GL048435
- Fasullo J (2004) A stratified diagnosis of the Indian Monsoon—Eurasian snow cover relationship. *J Clim* 17:1110–1122. doi:10.1175/1520-0442(2004)017<1110:ASDOTI>2.0.CO;2
- Fasullo J, Webster PJ (2003) A hydrological definition of Indian monsoon onset and withdrawal. *J Clim* 16:3200–3211. doi:10.1175/1520-0442(2003)016<3200a:AHDOIM>2.0.CO;2
- Flatau MK, Flatau PJ, Rudnick D (2001) The dynamics of double monsoon onsets. *J Clim* 14:4130–4146. doi:10.1175/1520-0442(2001)014<4130:TDODMO>2.0.CO;2
- Fu X, Lee J-Y, Wang B et al (2013) Intraseasonal forecasting of the Asian summer Monsoon in four operational and research models. *J Clim* 26:4186–4203. doi:10.1175/JCLI-D-12-00252.1
- Goswami BN, Krishnan R (2013) Opportunities and challenges in monsoon prediction in a changing climate. *Clim Dyn* 41:1. doi:10.1007/s00382-013-1835-4
- Goswami BN, Xavier PK (2005) ENSO control on the south Asian monsoon through the length of the rainy season. *Geophys Res Lett* 32:L18717. doi:10.1029/2005GL023216
- Hahn DG, Shukla J (1976) An apparent relationship between Eurasian snow cover and Indian Monsoon rainfall. *J Atmos Sci* 33:2461–2462. doi:10.1175/1520-0469(1976)033<2461:AARBES>2.0.CO;2
- Jeong J-H, Linderholm HW, Woo S-H et al (2013) Impacts of snow initialization on subseasonal forecasts of surface air temperature for the cold season. *J Clim* 26:1956–1972. doi:10.1175/JCLI-D-12-00159.1
- Koster RD, Mahanama SPP, Yamada TJ et al (2010) Contribution of land surface initialization to subseasonal forecast skill: first results from a multi-model experiment. *Geophys Res Lett* 37:L02402. doi:10.1029/2009GL041677
- Kripalani RH, Kulkarni A, Sabade SS (2003) Western Himalayan snow cover and Indian monsoon rainfall: a re-examination with INSAT and NCEP/NCAR data. *Theor Appl Climatol* 74:1–18. doi:10.1007/s00704-002-0699-z
- Kripalani RH, Oh JH, Kulkarni A et al (2007) South Asian summer monsoon precipitation variability: coupled climate model simulations and projections under IPCC AR4. *Theor Appl Climatol* 90:133–159. doi:10.1007/s00704-006-0282-0
- Krishnamurti TN, Kumar TSVV, Mitra AK (2006) Seasonal climate prediction of Indian summer monsoon. In: Wang B (ed) *The Asian Monsoon*. Springer, Berlin, pp 553–583
- Kumar KK, Rajagopalan B, Hoerling M et al (2006) Unraveling the Mystery of Indian Monsoon failure during El Niño. *Science* 314:115–119. doi:10.1126/science.1131152
- Li J, Wang JXL (2003) A new North Atlantic oscillation index and its variability. *Adv Atmos Sci* 20:661–676. doi:10.1007/BF02915394
- Li C, Yanai M (1996) The onset and interannual variability of the Asian Summer Monsoon in relation to land–sea thermal contrast. *J Clim* 9:358–375. doi:10.1175/1520-0442(1996)009<0358:TOA IVO>2.0.CO;2
- Li J, Zhang L (2009) Wind onset and withdrawal of Asian summer monsoon and their simulated performance in AMIP models. *Clim Dyn* 32:935–968. doi:10.1007/s00382-008-0465-8
- Li J, Yu R, Zhou T (2008) Teleconnection between NAO and climate downstream of the Tibetan Plateau. *J Clim* 21:4680–4690. doi:10.1175/2008JCLI2053.1
- Molteni F, Stockdale T, Balmaseda M et al (2011) The new ECMWF seasonal forecast system (System 4). ECMWF Technical Memorandum 656. European Centre for Medium Range Weather Forecasts, England
- Orsolini YJ, Senan R, Balsamo G et al (2013) Impact of snow initialization on sub-seasonal forecasts. *Clim Dyn*. doi:10.1007/s00382-013-1782-0
- Pai DS, Sridhar L, Badwaik MR, Rajeevan M (2015) Analysis of the daily rainfall events over India using a new long period (1901–2010) high resolution (0.25° × 0.25°) gridded rainfall data set. *Clim Dyn* 45:755–776. doi:10.1007/s00382-014-2307-1
- Peings Y, Douville H (2010) Influence of the Eurasian snow cover on the Indian summer monsoon variability in observed climatologies and CMIP3 simulations. *Clim Dyn* 34:643–660. doi:10.1007/s00382-009-0565-0
- Prodhomme C, Terray P, Masson S et al (2015) Oceanic factors controlling the Indian summer monsoon onset in a coupled model. *Clim Dyn* 44:977–1002. doi:10.1007/s00382-014-2200-y
- Robock A (2003) Land surface conditions over Eurasia and Indian summer monsoon rainfall. *J Geophys Res*. doi:10.1029/2002JD002286



- Saha SK, Pokhrel S, Chaudhari HS (2013) Influence of Eurasian snow on Indian summer monsoon in NCEP CFSv2 freerun. *Clim Dyn* 41:1801–1815. doi:[10.1007/s00382-012-1617-4](https://doi.org/10.1007/s00382-012-1617-4)
- Saji NH, Goswami BN, Vinayachandran PN, Yamagata T (1999) A dipole mode in the tropical Indian Ocean. *Nature* 401:360–363. doi:[10.1038/43854](https://doi.org/10.1038/43854)
- Shaman J, Tziperman E (2005) The effect of ENSO on Tibetan Plateau snow depth: a stationary wave teleconnection mechanism and implications for the South Asian Monsoons. *J Clim* 18:2067–2079. doi:[10.1175/JCLI3391.1](https://doi.org/10.1175/JCLI3391.1)
- Sperber KR, Annamalai H, Kang I-S et al (2013) The Asian summer monsoon: an intercomparison of CMIP5 vs. CMIP3 simulations of the late 20th century. *Clim Dyn* 41:2711–2744. doi:[10.1007/s00382-012-1607-6](https://doi.org/10.1007/s00382-012-1607-6)
- Stockdale TN, Anderson DLT, Balmaseda MA et al (2011) ECMWF seasonal forecast system 3 and its prediction of sea surface temperature. *Clim Dyn* 37:455–471. doi:[10.1007/s00382-010-0947-3](https://doi.org/10.1007/s00382-010-0947-3)
- Trenberth KE (1997) The definition of El Niño. *Bull Am Meteorol Soc* 78:2771–2777. doi:[10.1175/1520-0477\(1997\)078<2771:TDOE NO>2.0.CO;2](https://doi.org/10.1175/1520-0477(1997)078<2771:TDOE NO>2.0.CO;2)
- Turner AG, Annamalai H (2012) Climate change and the South Asian summer monsoon. *Nat Clim Change* 2:587–595. doi:[10.1038/nclimate1495](https://doi.org/10.1038/nclimate1495)
- Turner AG, Slingo JM (2011) Using idealized snow forcing to test teleconnections with the Indian summer monsoon in the Hadley Centre GCM. *Clim Dyn* 36:1717–1735. doi:[10.1007/s00382-010-0805-3](https://doi.org/10.1007/s00382-010-0805-3)
- van den Hurk B, Doblas-Reyes F, Balsamo G et al (2012) Soil moisture effects on seasonal temperature and precipitation forecast scores in Europe. *Clim Dyn* 38:349–362. doi:[10.1007/s00382-010-0956-2](https://doi.org/10.1007/s00382-010-0956-2)
- Vitart F, Molteni F (2009) Dynamical extended-range prediction of early monsoon rainfall over India. *Mon Weather Rev* 137:1480–1492. doi:[10.1175/2008MWR2761.1](https://doi.org/10.1175/2008MWR2761.1)
- Wang B, LinHo (2002) Rainy season of the Asian–Pacific summer Monsoon\*. *J Clim* 15:386–398. doi:[10.1175/1520-0442\(2002\)015<0386:RSOTAP>2.0.CO;2](https://doi.org/10.1175/1520-0442(2002)015<0386:RSOTAP>2.0.CO;2)
- Wang B, Kang I-S, Lee J-Y (2004) Ensemble simulations of Asian–Australian Monsoon variability by 11 AGCMs\*. *J Clim* 17:803–818
- Wang B, Ding Q, Joseph PV (2009) Objective definition of the Indian summer Monsoon onset\*. *J Clim* 22:3303–3316. doi:[10.1175/2008JCLI2675.1](https://doi.org/10.1175/2008JCLI2675.1)
- Webster PJ, Magaña VO, Palmer TN et al (1998) Monsoons: processes, predictability, and the prospects for prediction. *J Geophys Res Oceans* 103:14451–14510. doi:[10.1029/97JC02719](https://doi.org/10.1029/97JC02719)
- Wheeler MC, Hendon HH (2004) An all-season real-time multivariate MJO index: development of an index for monitoring and prediction. *Mon Weather Rev* 132:1917–1932. doi:[10.1175/1520-0493\(2004\)132<1917:AARMMI>2.0.CO;2](https://doi.org/10.1175/1520-0493(2004)132<1917:AARMMI>2.0.CO;2)
- Xavier PK, Marzin C, Goswami BN (2007) An objective definition of the Indian summer monsoon season and a new perspective on the ENSO–monsoon relationship. *Q J R Meteorol Soc* 133:749–764. doi:[10.1002/qj.45](https://doi.org/10.1002/qj.45)
- Xu L, Dirmeyer P (2011) Snow-atmosphere coupling strength in a global atmospheric model. *Geophys Res Lett* 38:L13401. doi:[10.1029/2011GL048049](https://doi.org/10.1029/2011GL048049)
- Yanai M, Wu G-X (2006) Effects of the Tibetan Plateau. In: Wang B (ed) *The Asian Monsoon*. Springer, Berlin, pp 513–549
- Yuan C, Tozuka T, Miyasaka T, Yamagata T (2009) Respective influences of IOD and ENSO on the Tibetan snow cover in early winter. *Clim Dyn* 33:509–520. doi:[10.1007/s00382-008-0495-2](https://doi.org/10.1007/s00382-008-0495-2)
- Zhang H, Liang P, Moise A, Hanson L (2012) Diagnosing potential changes in Asian summer monsoon onset and duration in IPCC AR4 model simulations using moisture and wind indices. *Clim Dyn* 39:2465–2486. doi:[10.1007/s00382-012-1289-0](https://doi.org/10.1007/s00382-012-1289-0)
- Zhou L, Murtugudde R (2014) Impact of Northward-propagating intraseasonal variability on the onset of Indian Summer Monsoon. *J Clim* 27:126–139. doi:[10.1175/JCLI-D-13-00214.1](https://doi.org/10.1175/JCLI-D-13-00214.1)